Electronic Supplementary Material (ESI) for Journal of Materials Chemistry A.


# Supporting Information

## Biomass in situ converted Fe single atomic sites coupled with $Fe_2O_3$ clusters embedded in porous carbons for oxygen reduction reaction

Ying Lei*, Fuwen Yang, Huaming Xie, Yongpeng Lei*, Xingyong Liu, Yujun Si, Honghui Wang

**Electrochemical measurements**

All electrochemical measurements were achieved in a three-electrode electrochemical AUTOLAB system at 25 ℃ and the temperature was controlled by a thermostat water bath, using Pt wire and a Ag/AgCl with saturated KCl solution electrode as a counter electrode and the reference electrode, respectively. All of the potentials were converted to the reversible hydrogen electrode (RHE) referring to Nernst equation ($E_{vs\ RHE}=E_{vs\ Ag/AgCl}$ + 0.197+ 0.059 pH). The preparation of working electrode was put into effect as follows: the catalyst ink suspension was fabricated by mixing 2 mg catalysts with 10 μL Nafion solution dispersed in 0.5 mL of water-isopropanol solution with volume ratio of 3:1 for at least 2 h to form a homogeneous ink. For the rotate disk electrode (RDE) tests, 7μL of ink solution was dropped onto the glassy carbon electrode of 5 mm in diameter with a 0.14 mg $cm^{-2}$ loading for all samples. Preparing work for testing is to bubble $O_2/N_2$ into 0.1 M KOH at least 30 min to make sure the solution was saturated with the bubbled gases. Electrochemical ORR performance was characterized by LSV polarization curves conducted in 0.1 M KOH solution. The cyclic voltammograms (CVs) were measured in $N_2$ and $O_2$-saturated KOH solution with a scan rate of 50 mV $s^{-1}$. In order to detect the practical electrochemical active surface area, a CV method was used to estimate the double layer capacitance ($C_{dl}$).The corresponding linear sweep voltammetry polarization curves were obtained with a rotating speed range from 400 to 2025 rpm on RDE with a scan rate of 10 mV $s^{-1}$ in $O_2$-saturated 0.1 M KOH solution. What's more, the electron transfer number was derived from the Koutecky-Levich (K-L) equation:

$$\frac{1}{j} = \frac{1}{j_L} + \frac{1}{j_k} = \frac{1}{B\omega^{1/2}} + \frac{1}{j_k} \quad (1)$$

$$B = 0.2nFC_0(D_0)^{2/3}\,v^{-1/6} \quad (2)$$

$$j_k = nFkC_0 \quad (3)$$

where j is the measured current density, $j_k$ and $j_L$ corresponds to the kinetic and diffusion-limiting current densities, respectively; ω is the angular velocity of disk; n represents the electron transfer number; F is the Faraday constant (F =96485 C $mol^{-1}$); $C_0$ is the bulk concentration for $O_2$ ($1.2\times10^{-6}$ mol $cm^{-3}$) dissolved in 0.1M KOH; $D_0$ is the diffusion coefficient of $O_2$ in electrolyte solution; v is the kinematic viscosity of electrolyte(0.01 $cm^{-2}$ $s^{-1}$). In order to demonstrate the stability of the catalyst, we conducted the tests using current-time (I~t) chronoamperometric response methods at 1600 rpm with a potential of 0.6 V (vs. RHE). For clarifying the hydrogen peroxide yield and electron transfer number during the oxygen reduction reaction process, we also conducted related tests on the rotating ring disk electrode (RRDE). Comparing to the RDE tests, there is a little change about the drop-casted process, which drop 10 μL of ink solution on glassy carbon electrode of 5.61 mm with a 0.16 mg $cm^{-2}$ loading mass. For comparison, we also used commercial Pt/C catalyst as a reference. The corresponding electrochemical tests were same to the above descriptions.

For performance evaluation of the Zn-air batteries, the air electrode was produced by uniformly dropping the catalyst ink suspension onto carbon paper then drying it at room temperature for several hours. The mass loading was 1.0 mg $cm^{-2}$. A polished zinc foil was used as the anode. The assembled details can be seen from Figure S15. Subsequently, we conduct a test to evaluate the performance of home-made battery. In the discharge process, the oxygen were reduced and followed by chemical reaction with the metal dissolved in the electrolyte. Discharge polarization curves were investigated by LSV. Galvalnostatic discharge test of Zn-air battery were conducted at the current density of 10 mA $cm^{-2}$ over 15 h.

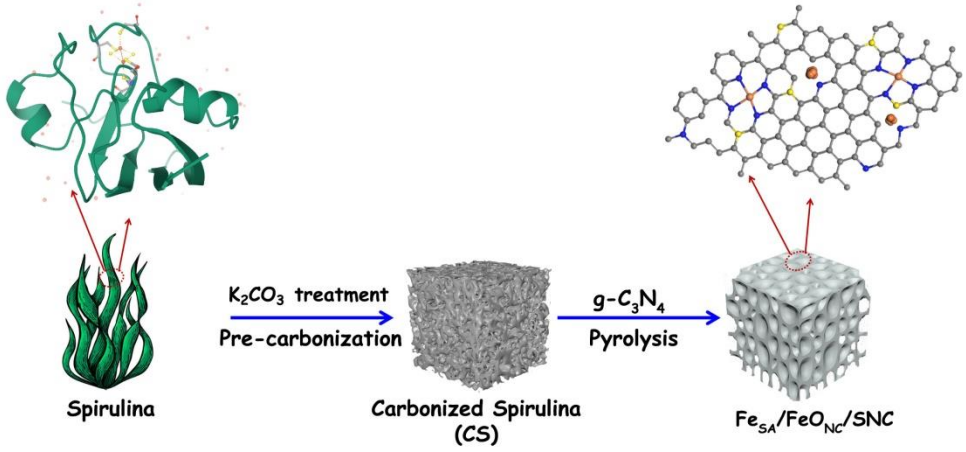


**Figure S1** Schematic for the synthesis of biomass spirulina-derived $Fe_{SA}/FeO_{NC}$/NCS sample.

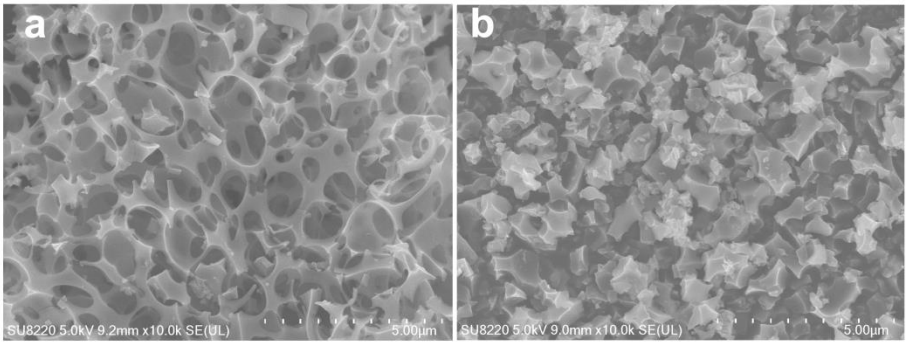


**Figure S2** SEM images of (a) CS and (b) $Fe_{SA}/FeO_{NC}$/NSC samples.

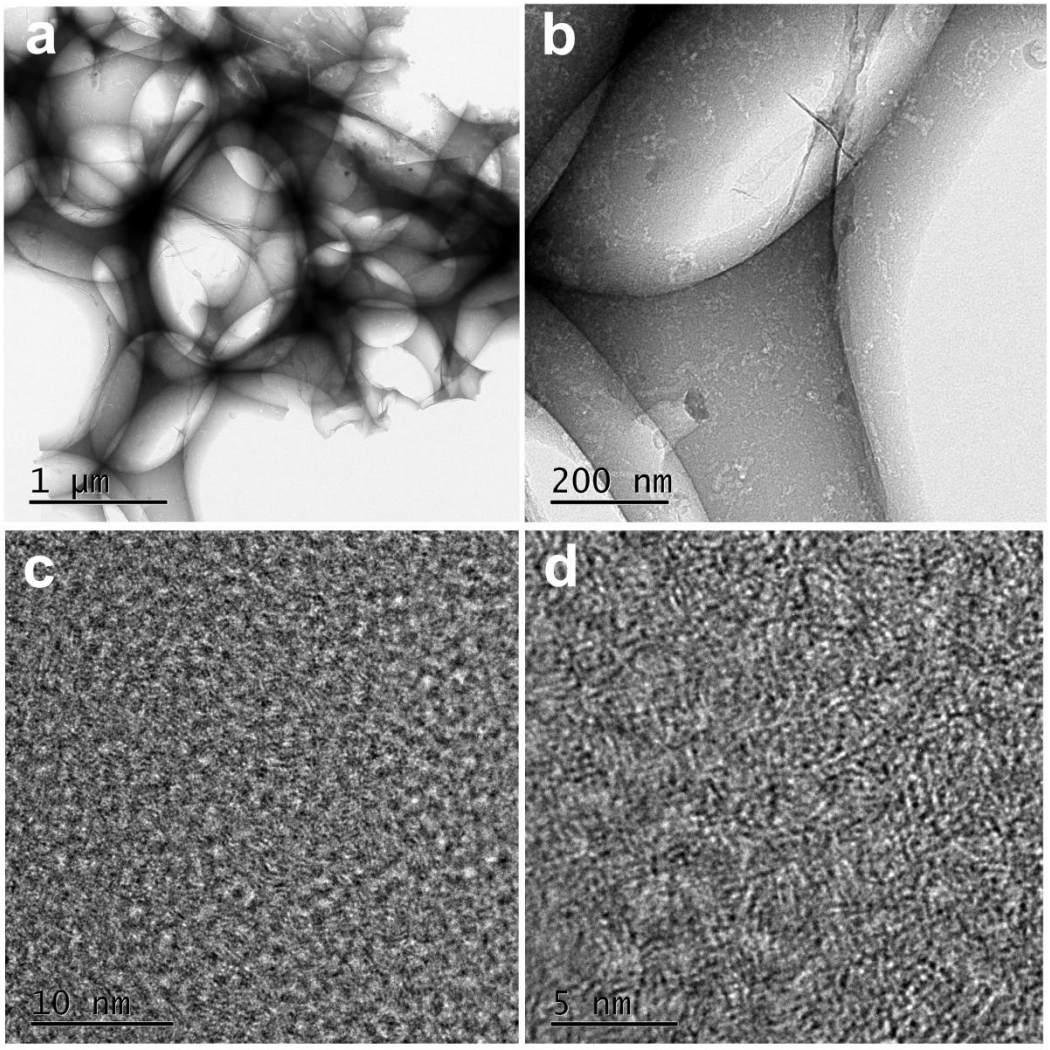


**Figure S3** TEM images and the corresponding HRTEM images of CS sample at different magnifications.

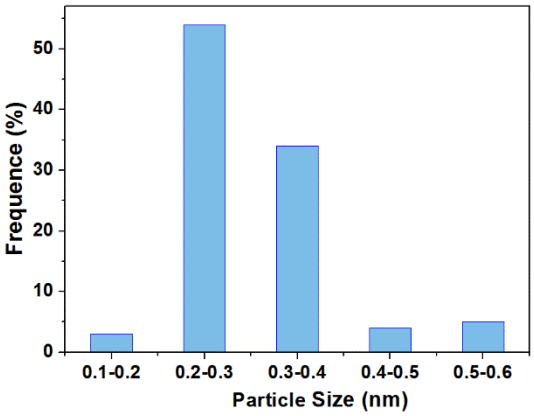


**Figure S4** Fe nanoclusters/particles size distribution of $Fe_{SA}/FeO_{NC}$/NSC according to HAADF-STEM images in Figure 1e.

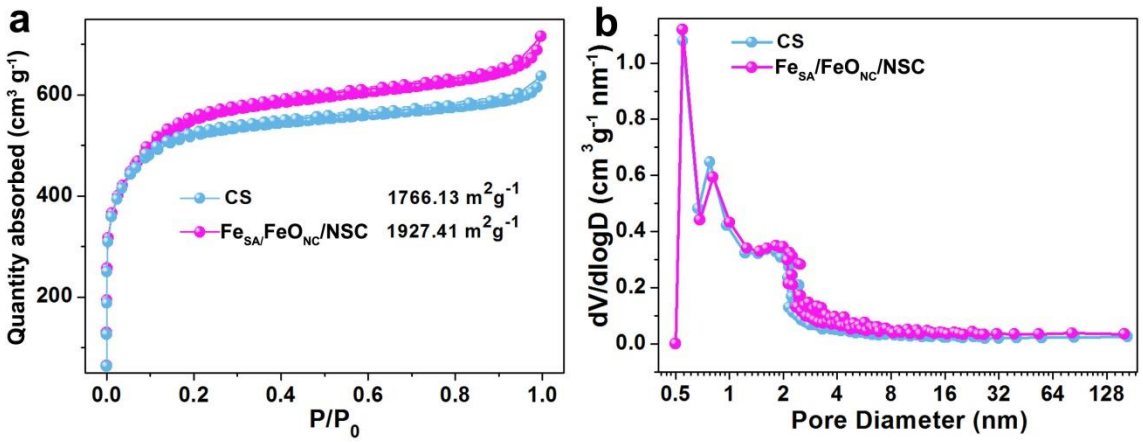


**Figure S5** (a) Nitrogen absorption desorption isotherms and (b) pore size distribution of CS and $Fe_{SA}/FeO_{NC}$/NSC.

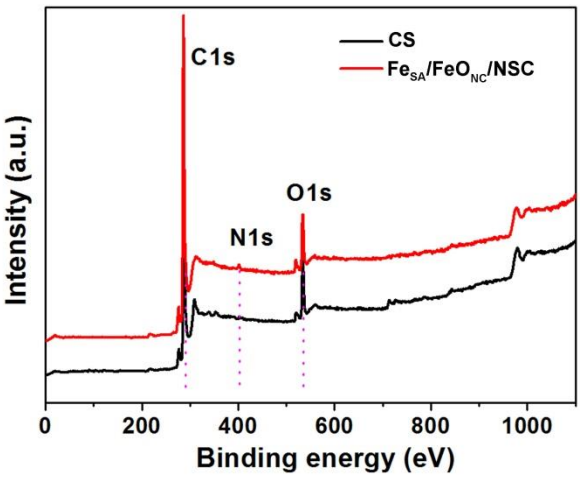


**Figure S6** XPS survey spectra of CS and $Fe_{SA}/FeO_{NC}$/NSC.

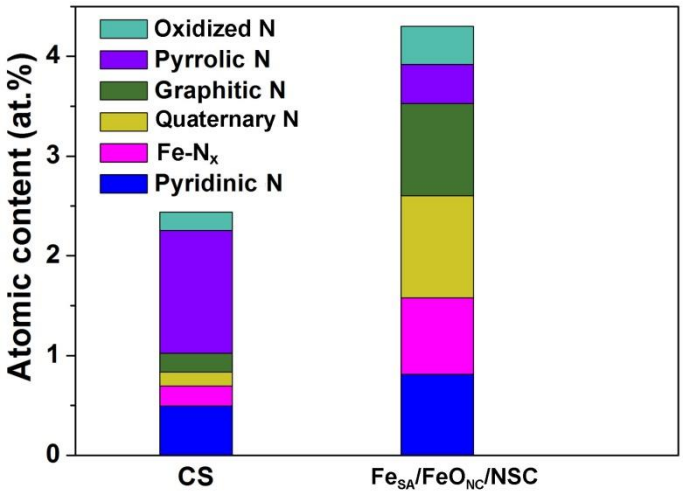


**Figure S7** The relative contents of different N species for CS and $Fe_{SA}/FeO_{NC}$/NSC based on their high-resolution N1s spectra.

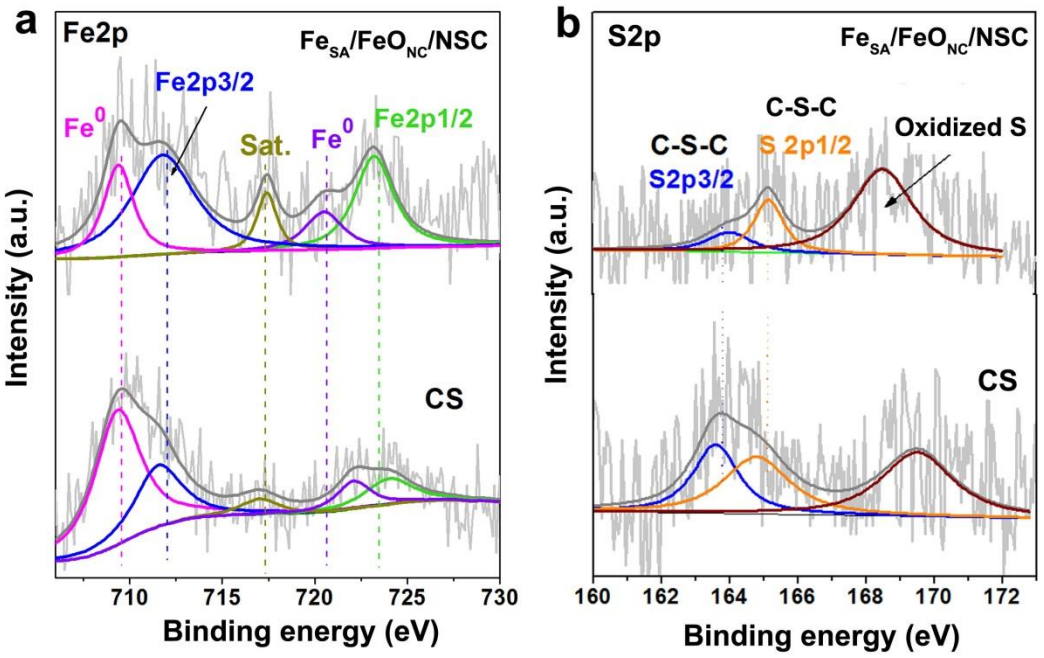


**Figure S8** (a) High-resolution Fe 2p, (b) S 2p spectra of CS and $Fe_{SA}/FeO_{NC}$/NSC, respectively.

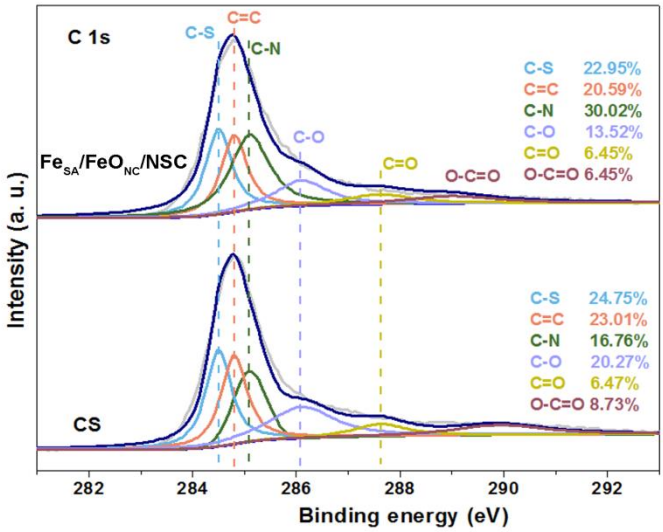


**Figure S9** High resolution C 1s spectra for CS and $Fe_{SA}/FeO_{NC}$/NSC.

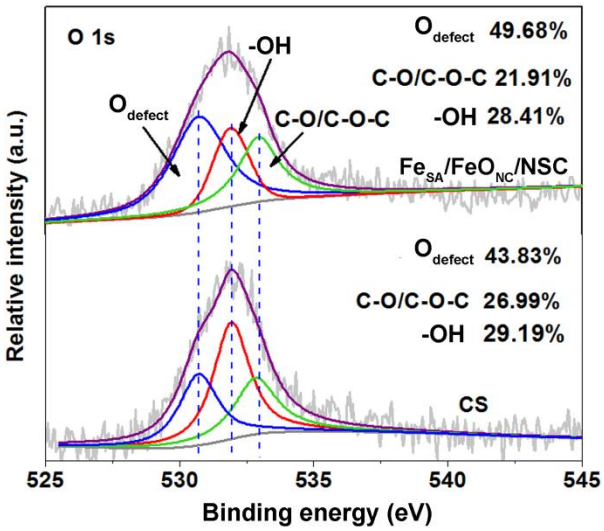


**Figure S10** High resolution O 1s spectra for CS and $Fe_{SA}/FeO_{NC}$/NSC.

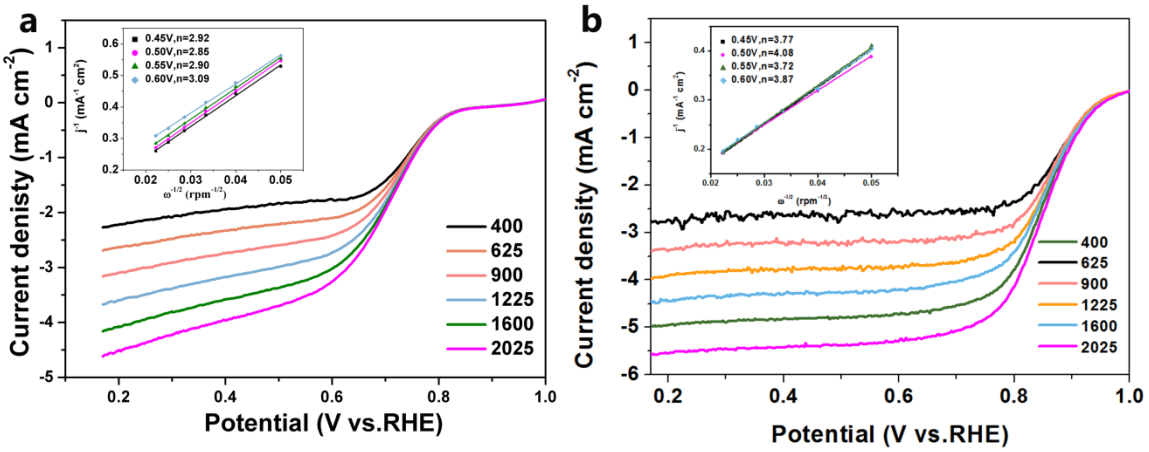


**Figure S11** LSV curves obtained at different rotating rate (inset: K-L plot) in 0.1 M KOH at 10 mV $s^{-1}$: (a) CS and (b) 20% Pt/C.

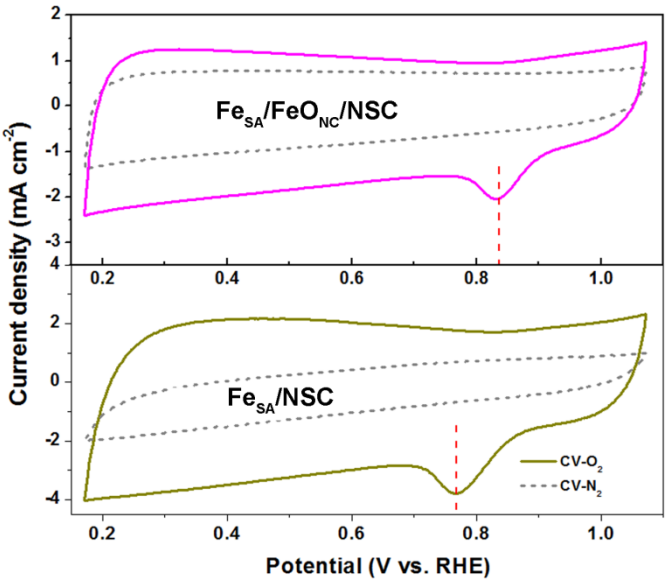


**Figure S12** CV curves for $Fe_{SA}/FeO_{NC}$/NSC and $Fe_{SA}$/NSC with HCl treatment in $O_2$-saturated 0.1 M KOH solution at the rotation speed of 1600 rpm (10 mV $s^{-1}$).

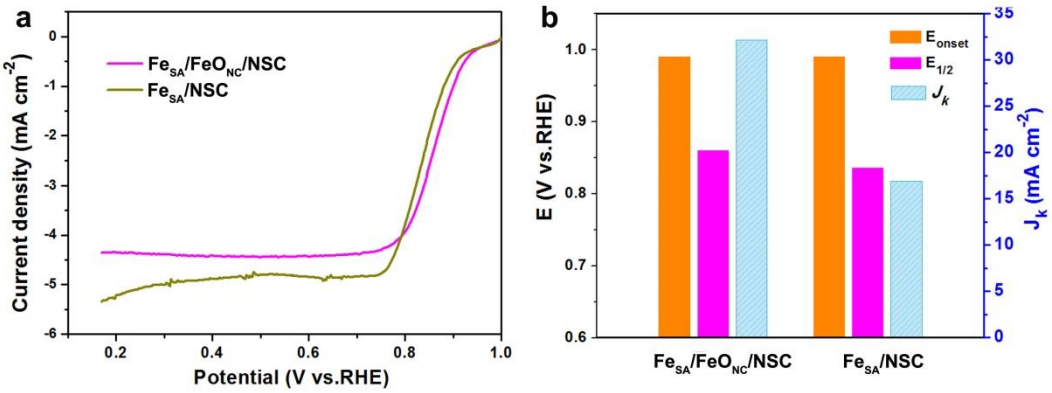


**Figure S13** (a) LSV curves for $Fe_{SA}/FeO_{NC}$/NSC and $Fe_{SAs}$/NSC with HCl treatment in $O_2$-saturated 0.1 M KOH solution at the rotation speed of 1600 rpm (10 mV $s^{-1}$), and (b) the comparison of their corresponding $E_{onset}$, $E_{1/2}$ and $J_k$ values.

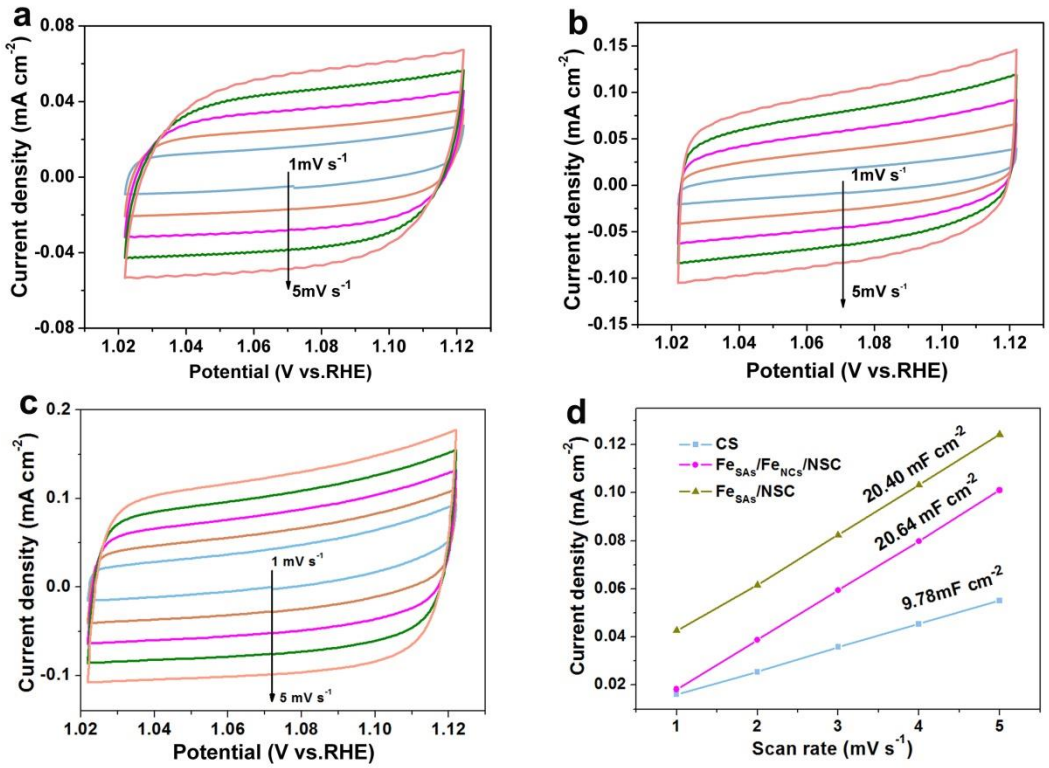


**Figure S14** Electrochemical CV of (a) CS, (b) $Fe_{SA}/FeO_{NC}$/NSC, (c) $Fe_{SAs}$/NSC and (d) the capacitive current measured at 1.07 V (vs. RHE) plotted as a function of scan rate (1~5 mV $s^{-1}$) of the as-prepared catalysts.

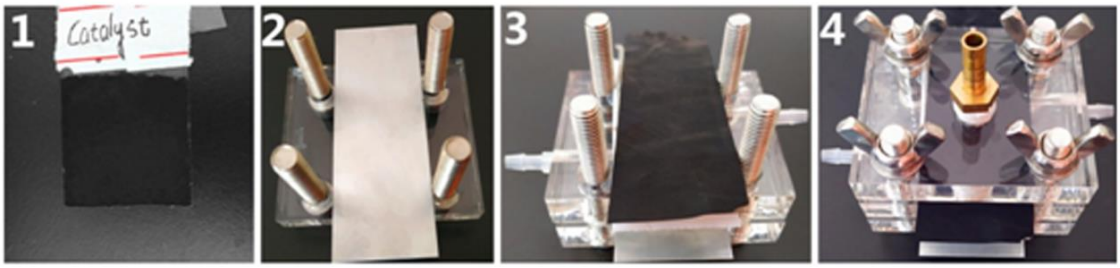


**Figure S15** The constructing process of home-made Zn-air battery.

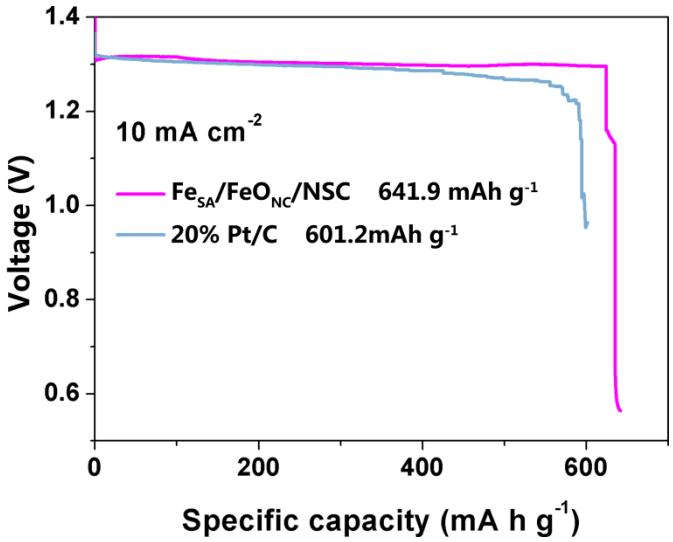


**Figure S16** Specific capacity plots of the Zn-air battery assembled with $Fe_{SA}/FeO_{NC}$/NSC and 20% Pt/C catalysts, respectively.

**Table S1** EXAFS fitting parameters at the Fe K-edge for various samples

| Sample | Shell | $N$ [a] | $R$ (Å) [b] | $\sigma^2$ (Å$^2$ ·10$^3$) [c] | $\Delta E_0$ (eV) [d] | $R$ factor (%) |
|---|---|---|---|---|---|---|
| FeACs/NSC | Fe-O | 3.9 | 1.94 | 8.0 | -2.0 | 0.6 |
| | Fe-S | 0.9 | 2.33 | 6.1 | 5.5 | |
| | Fe-O-Fe | 3.6 | 2.97 | 13.4 | -3.2 | |
| | Fe-O-Fe | 3.3 | 3.44 | 10.3 | | |

[a] $N$: coordination numbers; [b] $R$: bond distance; [c] $\sigma^2$: Debye-Waller factors; [d] $\Delta E_0$: the inner potential correction. $R$ factor: goodness of fit. $S$02 were set as 0.85/0.9, which were obtained from the experimental EXAFS fit of $Fe_2O_3$ reference by fixing CN as the known crystallographic value and was fixed to all the samples.

**Table S2.** Summary of the Mössbauer parameters and assignments to different iron species in $Fe_{SA}/FeO_{NC}$/NSC electrocatalyst.

| Fe species | IS ($mm\ s^{-1}$) | QS ($mm\ s^{-1}$) | Lw ($mm\ s^{-1}$) | Area %[a] | Content (%) | Assignment[b] |
|---|---|---|---|---|---|---|
| Sext1 | 0.48 | -0.171 | 0.582 | 5.7 | 26.71 | $Fe_2O_3$ [1] |
| Doublet 1 | 0.35 | 1.36 | 0.582 | 8.3 | 6.47 | $FeN_4$, LS [2, 3] |
| Doublet 2 | 0.32 | 0.81 | 0.58 | 66.6 | 51.76 | $X-Fe^{III}N_4-Y$, (X, Y = O/N ligands), HS [4, 5] |
| Doublet 3 | 0.32 | 2.530 | 0.582 | 19.4 | 15.06 | $Fe^{II}N_4$, like FePc, MS [6] |

[a] The relative absorption area of each iron species in $Fe_{SA}/FeO_{NC}$/NSC samples.

[b] LS, MS, and HS denote low-spin, medium-spin, and high spin, respectively.

**Table S3** A comparison of the electrocatalytic activities of the $Fe_{SAs}/Fe_{NCs}$/NSC catalyst and of the recently reported single atom catalysts

| Catalysts | $E_{1/2}$ (V *vs.* RHE) | Loading amount ($mg/cm^2$) | *Ref.* |
|---|---|---|---|
| $Fe_{SA}/FeO_{NC}$/NSC | 0.86 | 0.14 | **This work** |
| Co-POC | 0.83 | 0.10 | *Adv. Mater.*, 2019, **31**, 1900592. |
| $Fe_1$-HNC-500-850 | 0.842 | 0.20 | *Adv. Mater.*, 2020, **32**,1906905. |
| S, N-Fe/N/ C-CNT | 0.85 | 0.196 | *Angew. Chem.*, 2017, **56**, 610-614. |
| Fe-N/P-C-700 | 0.867 | 0.60 | *J. Am. Chem. Soc.*, 2020,**142**, 2404-2412 |
| CAN-Pc(Fe/Co) | 0.86 | 0.10 | *Angew. Chem.*, 2019, **131**, 14866-14872. |
| Mo SACs/N-C | 0.83 | 1.62 | *Nano Energy*, 2020, **67**, 104288. |
| N-Fe-SAs/N-C | 0.87 | 0.50 | *Nat. Commun.*, 2018, **9**, 5422. |
| FeAC@FeSA-N-C | 0.912 | 0.37 | *ACS nano*, 2019, **13**, 11853-11862 |
| $Fe{-}N_x{-}C$ | 0.91 | 0.30 | *Adv. Funct. Mater.*, 2019, **29**, 1808872. |

**Table S4** A comparison of the power density for zinc air battery with $Fe_{SA}/FeO_{NC}$/NSC as cathode with other single atoms-based catalysts reported recently.

| **Catalysts** | $E_{1/2}$ **(V *vs.* RHE)** | **Loading amount (mg/cm$^2$)** | ***Ref.*** |
|---|---|---|---|
| $Fe_{SA}/FeO_{NC}$/NSC | 0.86 | 0.14 | **This work** |
| Co-POC | 0.83 | 0.10 | *Adv. Mater.*, 2019, **31**, 1900592. |
| $Fe_1$-HNC-500-850 | 0.842 | 0.20 | *Adv. Mater.*, 2020, **32**,1906905. |
| S, N-Fe/N/ C-CNT | 0.85 | 0.196 | *Angew. Chem.*, 2017, **56**, 610-614. |
| Fe-N/P-C-700 | 0.867 | 0.60 | *J. Am. Chem. Soc.*, 2020,**142**, 2404-2412 |
| CAN-Pc(Fe/Co) | 0.86 | 0.10 | *Angew. Chem.*, 2019, **131**, 14866-14872. |
| Mo SACs/N-C | 0.83 | 1.62 | *Nano Energy*, 2020, **67**, 104288. |
| N-Fe-SAs/N-C | 0.87 | 0.50 | *Nat. Commun.*, 2018, **9**, 5422. |
| FeAC@FeSA-N-C | 0.912 | 0.37 | *ACS nano*, 2019, **13**, 11853-11862 |
| $Fe{-}N_x{-}C$ | 0.91 | 0.30 | *Adv. Funct. Mater.*, 2019, **29**, 1808872. |

## References


1. L. Zhong, C. Frandsen, S. Mørup, Y. Hu, C. Pan, L. N. Cleemann, J. O. Jensen and Q. Li, *Appl. Catal. B: Environ.*, 2018, **221**, 406-412.
2. U. I. Kramm, I. Herrmann-Geppert, J. Behrends, K. Lips, S. Fiechter and P. Bogdanoff, *J. Am. Chem. Soc.*, 2016, **138**, 635-640.
3. E. Kuzmann, Z. Homonnay, A. Mylonakis, H. Yin, Y. Wei, K. Kovács, S. Kubuki, Z. Klencsár, A. Vértes and A. Nath, *J. Phys.: Conf. Ser.*, 2010, **217**, 012029.
4. N. R. Sahraie, U. I. Kramm, J. Steinberg, Y. Zhang, A. Thomas, T. Reier, J.-P. Paraknowitsch and P. Strasser, *Nat. Commun.*, 2015, **6**, 1-9.
5. J. Li, S. Ghoshal, W. Liang, M. T. Sougrati, F. Jaouen, B. Halevi, S. McKinney, G. McCool, C. Ma and X. Yuan, *Energ. Environ. Sci.*, 2016, **9**, 2418-2432.
6. Y. Zhu, B. Zhang, X. Liu, D. W. Wang and D. S. Su, *Angew. Chem.*, 2014, **126**, 10849-10853.